ACS NANO

www.acsnano.org

ARTICLE

Low-Voltage Haze Tuning with Cellulose-Network Liquid Crystal Gels

Souvik Ghosh,* Eldho Abraham, and Ivan I. Smalyukh*

Cite This: https://doi.org/10.1021/acsnano.3c03693

Read Online

ACCESS | Metrics & More | Article Recommendations | Supporting Information

ABSTRACT: Being key components of the building envelope, glazing products with tunable optical properties are in great demand because of their potential for boosting energy efficiency and privacy features while enabling the main function of allowing natural light indoors. However, windows and skylights with electric switching of haze and transparency are rare and often require high voltages or electric currents, as well as not fully meet the stringent technical requirements for glazing applications. Here, by introducing a predesigned gel material we describe an approach dubbed "Haze-Switch" that involves low-voltage tuning of the haze coefficient in a broad range of 2−90% while maintaining high visible-range optical transmittance. The approach is based on a nanocellulose fiber gel network infiltrated by a nematic liquid crystal, which can be switched between polydomain and monodomain spatial patterns of optical axis via a dielectric coupling between the nematic domains and the applied external electric field. By utilizing a nanocellulose network of nanofibers ∼10 nm in diameter we achieve <10 V dielectric switching and <2% haze in the clear state, as needed for applications in window products. We characterize physical properties relevant to window and smart glass technologies, like the color rendering index, haze coefficient, and switching times, demonstrating that our material and envisaged products can meet the stringent requirements of the glass industry, including applications such as privacy windows, skylights, sunroofs, and daylighting.

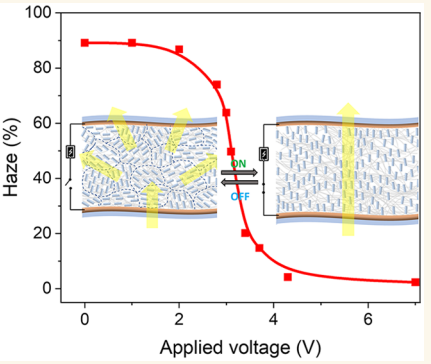

KEYWORDS: *smart windows, cellulose nanofibers, nanoporous network, liquid crystals, emergent nematic domains, ultrahigh haziness*

INTRODUCTION

Gels are an important class of soft matter systems that are composed of a liquidlike or gaslike medium entrapped in a three-dimensional cross-linked host network. Their physical characteristics are determined by their arrangement and composition at mesoscale. The structural variation in gels leads to tunable light propagation effects which is ideal for designing light−matter interaction and, overall, its bulk optical behavior.[1] The complex light scattering arising from nano- to micrometer-sized structures in composite systems allows for adjustable optical transparency in the visible and near-infrared (NIR) wavelengths while maintaining high overall transmission.[2,3] This is crucial for studying fundamental light transport effects in disordered media[4−6] as well as useful for diverse optical applications[7−9] and boosting the efficiency of optoelectronic devices.[10−12] These scientific and technological pursuits necessitate switchable optical haze without suffering from optical energy loss associated with, for example, absorption. Hence, ubiquitous control on local structure and composition in disordered medium including gels and composites is highly desired, which is able to selectively influence the optical diffusion of the transmitted light while ensuring unimpeded total light transmission. In this regard, electrically induced effects provide fast, robust, and dynamic control of materials properties that, in turn, modulate the optical behavior of a system, albeit alternative methods based on thermal, optical, and humidity-triggered stimulations offer only passive operation.[13] On the other hand, mechanical actuation is another promising alternative that can function without external energy input. However, integrating mechanochromic materials into existing architectural systems can be quite arduous due to the requirement of large strain for optical modulation.[14] Especially, uniform straining over a large scale is highly challenging, which can increase complexity in design. Also, repeated and prolonged mechanical strain can lead to degradation in mechanoresponsive optical performance and durability.

Despite several emerging materials and technologies, possibilities to actively manipulate the ensuing optical

Received: April 25, 2023
Accepted: September 8, 2023

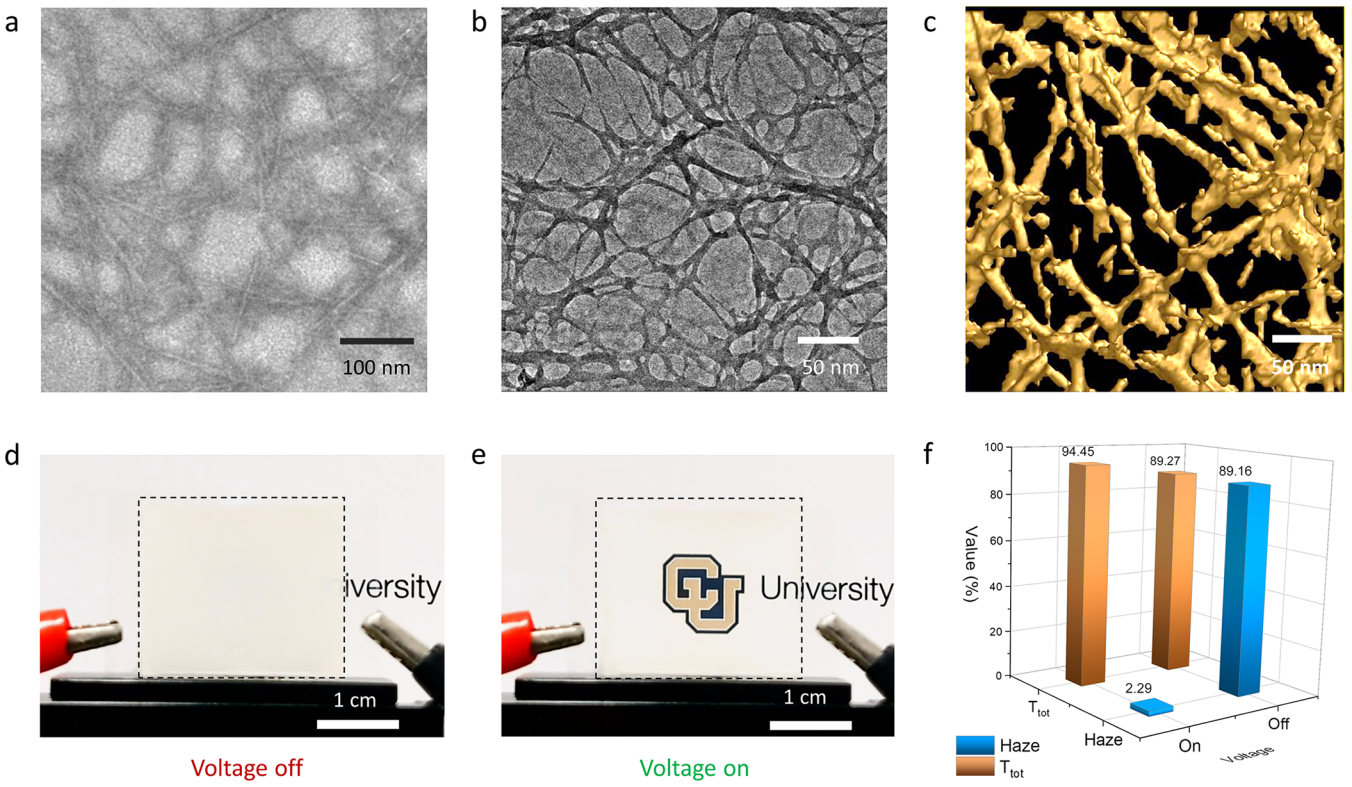

Figure 1. Fabrication of the CNLC gel and demonstration of haze switching. (a) Transmission electron microscopy (TEM) image of individualized TEMPO-oxidized cellulose nanofibers negatively stained with 1% phosphotungstic acid solution. (b) TEM image of the cross-linked network of nanofibers. (c) Tomographic TEM visualization of the network showing the porous structure. (d, e) CNLC in opaque and transparent states with the CU logo placed behind the cell, without and with applied voltage. (f) Comparison of the haze coefficient and total visible transmission of the CNLC cell with and without applied voltage. The copyright of the logo of CU used in this figure belongs to the University of Colorado at Boulder and is permitted for use in this publication.

properties in gel-like systems are still limited, rarely scalable, and often require high electrical energy input, which are widely recognized technological challenges.[13,15] Although high transmission and high haze properties have been achieved simultaneously in conventional gel-like materials developed from isotropic constituents, however, so far only in a static manner,[16−18] a suitable composition with optically anisotropic materials promises to enable orientation-dependent properties that can be regulated externally with weak stimuli like fields. In this direction, gel materials with combinations of an isotropic host network and anisotropic guest liquid or vice versa have been investigated, where one of the components is optically anisotropic. For example, a cross-linked network of birefringent cellulose nanofibers infiltrated by isotropic fluids like air and water results in aerogels[19,20] and hydrogels[21,22] with anisotropic physical and optical properties. Subsequently, the integration of anisotropic fluids such as liquid crystals (LCs) into networks of amorphous polymers forms composites whose properties can be modulated by using electrical stimulation. Until now, electrically driven dynamic optical scattering from the polymer−liquid crystal (P-LC) composite materials has been the most successful approach for regulating optical transparency with reduced optical scattering losses in the visible and NIR wavelengths.[15,23−25] The fast rotation of the LC director (average orientation of rod-like LC molecules) with respect to the applied electric field in different types of LC-based composites including polymer-dispersed liquid crystals (PDLCs),[26,27] polymer-stabilized liquid crystals (PSLCs),[28−30] polymer-stabilized cholesteric textures (PSCTs),[31] and nematic gels with aligned network of fibers[32,33] offers a fast and consistent optical response, which is necessary for practical applications. The robust and reliable modulation of optical transparency in P-LC composite materials has shown potential impacts in diverse optical technologies ranging from smart windows[15,34,35] and information displays[36−38] to vision therapy,[39,40] optical security devices,[41] and many more.[42,43] Yet, electrical switching in P-LC composites, including the commercially available PDLCs, suffers from the requirement of a high driving voltage, which is a key limiting factor for smart glass applications, especially in terms of power efficiency and both costs and safety considerations associated with high-voltage wiring of window units. These fundamental problems, along with the challenges of scalable, cost-effective manufacturing, have hindered the widespread adoption of P-LC materials for building-envelope technological applications.[15,24] Similar drawbacks also exist in alternate modes for controlling optical transmission with electrochromic materials and suspended particle devices.[13] These methods provide a broad-band optical response covering UV to vis-NIR wavelengths but rely primarily on absorption mechanisms for optical tunability. They also have a significantly slower response time (several minutes) as well as higher cost and energy input compared to those of LC-based systems. In recent years self-powered devices that rely on energy-harvesting technologies such as solar cells,[44] triboelectric nanogenerators,[45−47] and droplet-based electricity generators[48] have been explored for P-LC switching. These mechanisms show great promise in providing the required high

https://doi.org/10.1021/acsnano.3c03693
ACS Nano XXXX, XXX, XXX−XXX

voltage for modulating P-LC optical characteristics without the consumption of conventional electrical energy. Despite that, apart from additional cost and integration complexities, these self-powering mechanisms have some basic limitations that depend on several external factors such as weather conditions, pollution concerns, the requirement of continuous and large input of external forces, mechanical abrasions during running, etc. The challenge that emerges is, therefore, how to achieve a lossless composite material with tunable optical properties and that has the potential for scalable as well as cost-effective manufacturing, enabling low-voltage manipulation of haze, without compromising the essential qualities of smart glazing, i.e. simple operation, customer safety, fast response, color-neutral appearance, independence from light polarization, and durable switching cycles. Most importantly, such an operation has never been combined with the demonstration of a low-haze clear window state being switched to a high-haze daylighting state of glazing, despite being in great demand.

Here, by weakly coupling nematic LC molecules to a cross-linked three-dimensional network of ultrathin anisotropic cellulose nanofibers (CNF), we introduce a haze-switch technology with substantial power efficiency, high visible-range transmittance, and material properties adequate for smart-glass-related applications. The ensuing cellulose-network liquid crystal (CNLC) gel exhibits electro-optic characteristics that enable facile control of light−matter interaction, demonstrating large transparency tunability (∼90%) within a millisecond time scale while maintaining high overall transmission (>90%) at a low operating voltage (∼3−5 V), consuming at least 100 times less electrical power than conventional P-LC-based composites. The observed threshold characteristics and the emergence of micrometer-scale nematic domains that lead to dynamic optical response have been explained with phenomenological model accounting for the elastic, dielectric, and surface anchoring properties of LCs. The anchoring energy estimated from modeling closely correlates with the experimental findings, thereby confirming weak-boundary-coupling conditions which are highly sought after in switchable composite LC gels. We discuss how our optically anisotropic constituents within the mesostructured CNLC gel produce strong optical scattering from electrically controlled spatially varying optical inhomogeneities arising from anisotropic optical interactions of the gel with spatially varying optical axis orientations. We demonstrate how a state with high optical haze (∼90%) is switched to a low-haze (∼2%) state within over 10^4 operating cycles without performance degradation, with the overall functioning of the CNLC gel in both states being uniform, color-neutral, and independent of light polarization. Our approach, dubbed "Haze-Switch", promises technological utility in many glazing products ranging from privacy windows to daylighting.

RESULTS AND DISCUSSION

For the fabrication of the CNLC cell, at first, the CNFs are synthesized by oxidation of natural cellulose derived from wood pulp using 2,2,6,6-tetramethylpiperidine-1-oxyl (TEMPO) radicals[49,50] (described in detail in Methods). The choice of nanocellulose as a host matrix for the LC fluid is well justified, not only for its natural abundance, low-cost fabrication, and intrinsic sustainability but also for its excellent mechanical flexibility for scalable manufacturing, ultrahigh optical transparency, and strong optical anisotropy.[18,51,52] The as-synthesized nanofibers are hundreds to thousands of nanometers long with a diameter of only about 3−6 nm (Figure 1a) and exhibit crystalline structures and birefringence. They are stably dispersed in water as individual fibers by exploiting the electrostatic repulsion of their surface charges associated with carboxylate anions. In our study, an aqueous dispersion of such CNFs is mixed with silica spacers with micrometer-range diameters (which will define the gap thickness between the glass substrates) and placed between two substrates. Upon cross-linking of the fibers by hydrogen bonding between carboxyl groups, a 3D network forms, as shown in Figure 1b. The 3D network of cellulose nanofibers is highly porous with a randomly distributed irregular pore size (Figure 1c). Finally, the CNLC is formed after infiltrating the network with a small-molecule thermotropic LC, 4-cyano-4′-pentylbiphenyl (5CB), that follows multiple solvent exchange steps (see Methods for details). The as-prepared CNLC gel has a hazy appearance due to the combined effect of multiple scattering effects described below.

Inside the CNLC gel, the emergent microscopic domains (discussed later) of spatially varying director orientation and refractive index appearing from the weak interaction between the CNFs and LC molecules function as tunable light-scattering centers. These domains and the domain walls in between are the main sources of haze. Furthermore, the substantial difference in refractive indices between LC and CNF leads to opaqueness. The CNFs consist of both amorphous and crystalline regions, with the latter exhibiting anisotropic polarization-dependent refractive indices so that the effective refractive index properties also depend on the degree of crystallinity. A CNF fiber with a higher crystallinity has a high refractive index. For ideally oriented crystallites under perpendicularly incident illumination, the refractive indices were reported to be $n_e^{CNF} \approx 1.618$ for light polarization along the fiber and $n_o^{CNF} \approx 1.544$ when light is polarized perpendicular to the fiber axis, where n_e and n_o are the extraordinary and ordinary refractive indices, respectively.[53] Considering the slightly imperfect cellulose crystallite orientation and coexisting amorphous contents with ∼74% crystallinity of the TEMPO-oxidized cellulose nanofibers (TOCN),[50] the refractive index is estimated[54] to be $n_e^{TOCN} \approx 1.59$ and $n_o^{TOCN} \approx 1.53$. Also, as reported in the literature,[50] for a TOCN thin film the average refractive index was found to be, $n_{avg}^{TOCN} = 1.545 \pm 0.002$, which closely agrees with the estimated value ($n_{avg}^{TOCN} = \frac{n_e^{TOCN} + n_o^{TOCN}}{2} \approx 1.56$). On the other hand, 5CB in its nematic phase (at temperatures below 35 °C) is also a birefringent optical material having distinct refractive indices along its long and short axis. For 5CB, the extraordinary refractive index is $n_e^{5CB} = 1.716$ and the ordinary refractive index is $n_o^{5CB} = 1.531$, at 589 nm and 25 °C.[54] As a result, when unpolarized light passes through the randomized network, depending on the light polarization and orientation of nematic domains, a strong mismatch of refractive indices (0.2−0.1) and their spatial inhomogeneity produce a large scattering of light in the CNLC film. Additionally, fluctuations in the director orientation within the nematic state of 5CB also play a role in scattering, although this contribution is relatively small for the used thicknesses of the CNLC layers. The as-prepared CNLC gel can be electrically switched when sandwiched between two substrates having inner surfaces coated with transparent and conductive indium tin oxide (ITO). This switching of LC molecules happens because of their dielectric coupling to the applied electric field. Initially, in the voltage-off

https://doi.org/10.1021/acsnano.3c03693
ACS Nano XXXX, XXX, XXX−XXX

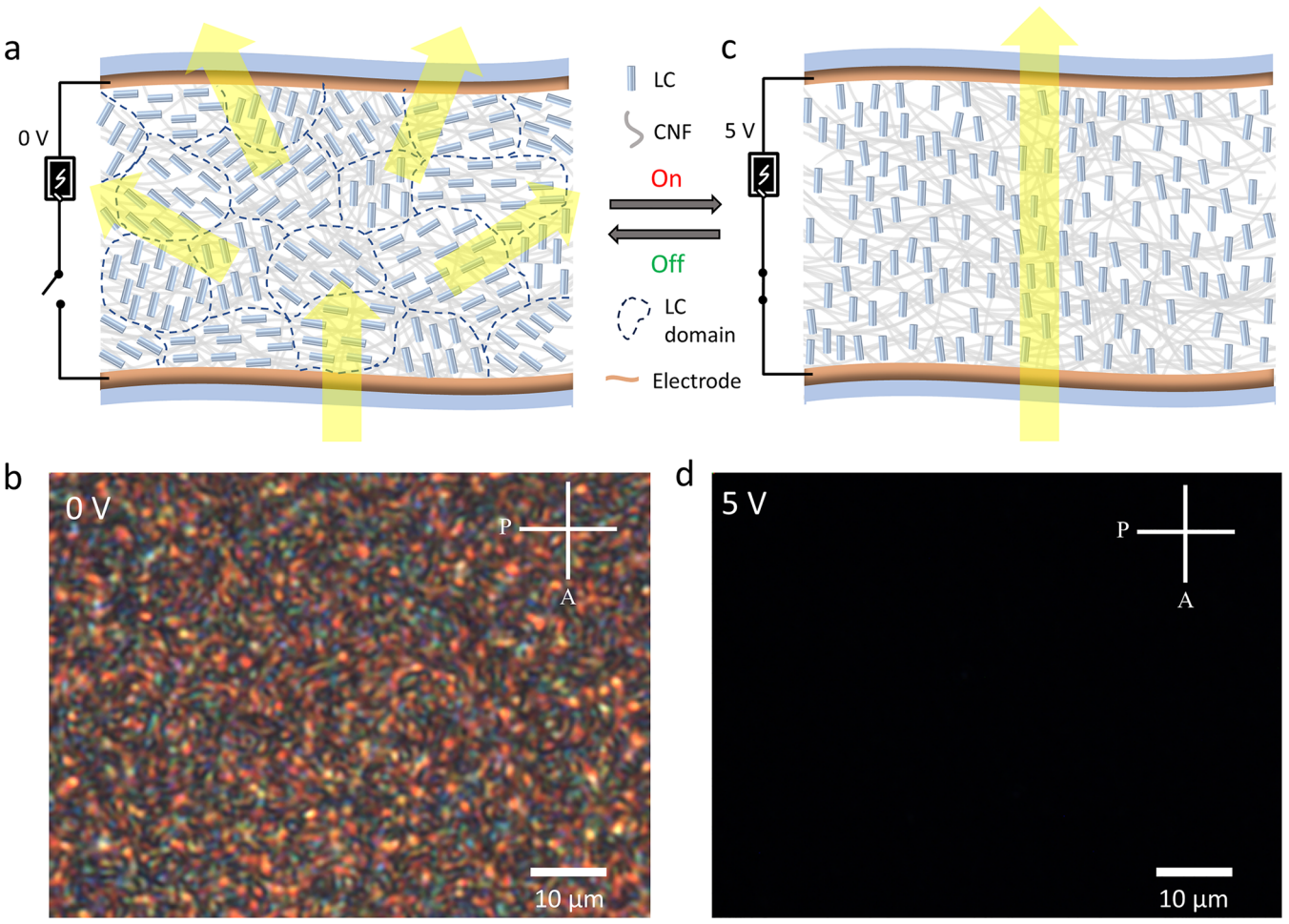

Figure 2. Mechanism of reversible haze switching. (a) Schematic illustration of emerging domains larger than the pores of the CNF network and associated scattering of incident illumination from the nonhomogeneous, multidomain gel in the default state. The figure is not to scale. (b) Optical microscopy image of CNLC without voltage under crossed polarizers showing micrometer-sized LC domains. (c) Schematic demonstration of the low-voltage transition of CNLC gel to a homogeneous transparent state due to realignment of LC domains under an external electric field. The figure is not to scale. (d) Polarized optical microscopy image of CNLC gel at 5 V.

state, the CNLC film appears opaque at room temperature, obscuring its background (see Figure 1d). Upon application of voltage, the optical axis of the positively anisotropic LC material rotates and gets oriented vertically to the substrate, uniformly across the cell, while following the applied electric field. With the composite design under an appropriate choice of the LC material that matches the refractive index of the CNF film, the gel scatters light minimally and becomes transparent, clearly displaying the image (University of Colorado logo) in its background (see Figure 1e). Once the applied field is removed, the surface interactions return the nematic LC to its randomly aligned opaque state. A demonstration of the transparency-switching CNLC smart glass, changing between the hazy OFF-state and transparent ON-state multiple times, is also shown in Video S1, which confirms the fully reversible and repetitive nature of the electric switching mechanism. The measured contrast in the haze coefficient $\Delta H \approx 87\%$ and total visible transmittance $\Delta T_{tot} \approx 5\%$, before and after application of voltage, is shown in Figure 1f. This finding illustrates the haze-switching concept, which provides the transparency-tuning capability of the CNLC gel while offering high overall light transmittance maintained in both the transparent and opaque states.

Figure 2 reveals and illustrates the switching mechanism of the CNLC cell without and with applied voltage. Inside the network of CNFs, the LC free energy has contributions from both bulk elastic free energy (F_b) associated with director deformations and surface energy (F_s), which scale as KR and WR^2, respectively, where K is the average Frank elastic constant, W is the surface anchoring strength, and R is the effective dimension. The ratio of these two energies F_s/F_b yields R/l_e, where $l_e = K/W$ is the de Gennes-Kléman extrapolation length. For LC in composite systems with a randomly oriented network, the competition between F_s and F_b determines the equilibrium molecular arrangements. Therefore, under a weak surface anchoring condition in small domains, bulk elastic effects dominate. If the characteristic length of the network (i.e., pore size) L is smaller than l_e, then the energetically favorable arrangement is the one that reduces the bulk elastic energy F_b to a minimum. As the nematic subsystems are interconnected, the elastic energy reduced is greater than the energy increased due to the surface misalignment. Consequently, the director field can achieve uniformity across lengths larger than the typical pore size L of the CNLC network. In our system, the extrapolation length l_e is on the order of a micrometer arising from the weak surface anchoring strength (discussed later) of the network. For $L < l_e$,

https://doi.org/10.1021/acsnano.3c03693
ACS Nano XXXX, XXX, XXX−XXX

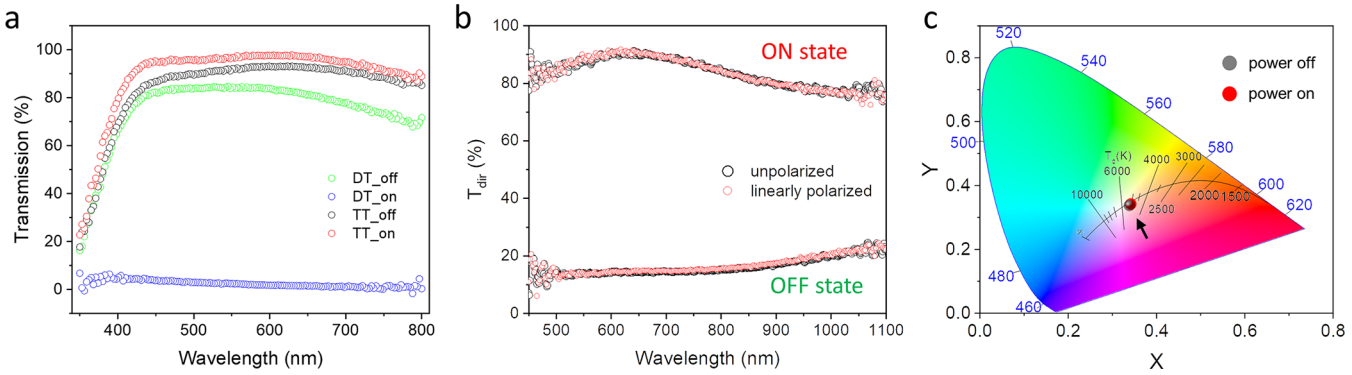

Figure 3. Optical properties of the CNLC gel . (a) Dependence of total (TT) and diffuse (DT) transmittance in CNLC gel in the visible spectral range, with and without voltage. (b) Spectral dependence of direct transmission using unpolarized and linearly polarized light with and without voltage. (c) Perceived color and color temperature of the CNLC gel placed between two glass substrates coated with ITO represented on the CIE1931 chromaticity diagram. A black arrow marks the location of color coordinates on the diagram.

a typical domain size can be estimated from the analytical expression[55] $R/l_e \approx L/l_e + l_e/L$, considering the random-field arguments of Imry and Ma.[56] Taking a typical pore size $L \approx$ 100−200 nm, the average domain size R is found to be around 5−10 μm. We note that because of the simplifying assumptions, the approximate values of R must be considered as order-of-magnitude estimates only. Domains with similar micrometer length scales indeed have been observed experimentally (see Figure 2b), in accordance with the Imry−Ma argument that explains the instability of an ordered state of a very large system against a random field even if that is much weaker than the interactions favoring the ordering. Due to the existence of weak and random surface interactions, the long-range nematic order is split into nematic domains of size R, which is larger than the typical pore dimensions of the network as shown schematically in Figure 2a. The LC director therefore forms irregularly aligned polydomain structure with microscale domains impacted by the TOCN network but does not follow their alignment locally. These emerging microscopic domains of randomly oriented director and spatially varying refractive index work as light-scattering centers. In addition, the refractive index contrast between the fibers and LC domains as well as the LC director fluctuations strongly diffuse the light propagating through the gel.[49] Subsequently, with the application of voltage between the ITO surfaces, the CNLC switches to a transparent state. Reacting to the applied voltage, the director and molecules of 5CB with strong positive dielectric anisotropy reorient themselves vertically, following the electric field. This results in the extinction of light under crossed polarizers (Figure 2d). Therefore, in the ON state, only the ordinary refractive index of 5CB becomes relevant as the LC director becomes parallel to the light propagation direction under normal incidence, yielding nearly matching refractive indices ($n_{avg}^{TOCN} - n_o^{5CB} \approx 0.01$) between the TOCN film and the surrounding LC medium with vertically aligned 5CB molecules. Consequently, the nematic domains of the randomly oriented director and spatially varying refractive index disappear, turning the CNLC into a clear, homogeneous optical medium, thereby hugely reducing the scattering, as illustrated in Figure 2c. Additionally, in the presence of the applied field, the director fluctuations of 5CB medium are partly suppressed, also leading to lower scattering. As a result, as shown in Figure 3a, in the ON state, the CNLC cell shows very high transparency in the visible wavelengths. A UV−vis spectrophotometer with a reliable detection range of 350−800 nm is used for measuring total and diffused transmittance, revealing changes of transmission and haze with switching. In the transparent mode, only a fraction of incident light gets scattered effectively, giving a weak diffused transmission T_{dif} = 2.1%. The nature of this weak light scattering in the clear state is mainly Rayleigh-type as observed from the stronger scattering at short wavelengths compared to longer wavelengths. On the other hand, when the voltage is turned off, the light diffusion jumps up to T_{dif} = 79.6%, turning the cell opaque almost instantaneously, but the overall transmittance drops only slightly to T_{tot} = 89.27%. From the presence of large scattering LC domains that are comparable to or larger than the incident light wavelengths, most of the incident light gets scattered along the forward direction, which is consistent with Mie-type scattering. We also tested the CNLC cell under polarized illumination as shown in Figure 3b. To characterize any effect of incident light polarization even on the microscopic scale, the direct optical transmission of a tiny region of the sample was collected using a microscope and analyzed with a portable spectrometer mounted on it. Over a broad range of wavelengths from 400 to 1100 nm, the optical response under polarized light remains nearly identical to that of unpolarized illumination. This confirms that the optical tunability is independent of light polarization for normally incident light, differently from gels with orientationally aligned fibers that scatter light depending on the direction of polarization leading to a reduced optical contrast.[32,57] Therefore, the CNLCs can be effectively used for applications under ambient light without requiring any polarizing optical elements. Another key factor for practical applications is the color-neutral appearance of the cell. To quantify that, we determined color perception indices using the CIE 1931 *xy* color space, which is intended to depict visual color perception of the human eye. By analyzing the transmitted light from the CNLC cell we obtain chromaticity coordinates of (0.33958, 0.34111) for the OFF state, that changes only marginally to (0.3365, 0.33697) when the cell is switched fully. In both scenarios, the chromaticity coordinates are positioned within the gray area of the diagram (Figure 3c), indicating exceptional color neutrality.

To characterize the switching behavior of the CNLC cell in response to the applied field, the sample is examined using polarized-light optical microscopy by keeping the CNLC cell between two crossed polarizers (Figure S1). Initially, in the voltage-off state, the gel appears bright as the light passing

https://doi.org/10.1021/acsnano.3c03693
ACS Nano XXXX, XXX, XXX−XXX

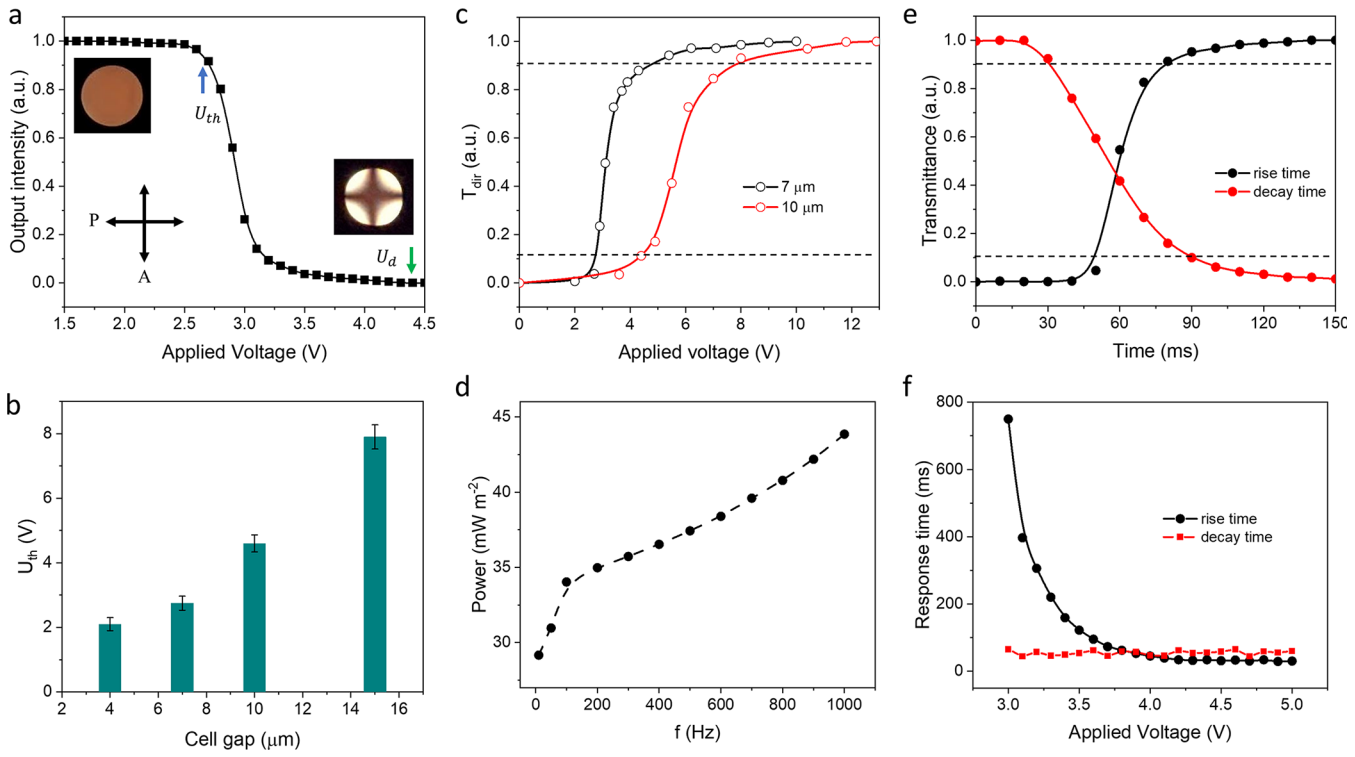

Figure 4. Electro-optic response of the CNLC gel. (a) Transmission of light through the crossed polarizers as a function of applied voltage at 1 kHz for a 7 μm thick CNLC cell. The blue and green arrows indicate the threshold voltage U_{th} and driving voltage U_d, respectively. The conoscopic images corresponding to 0 and 5 V are shown in the inset. (b) Threshold voltage vs cell thickness plot. (c) Direct transmission vs applied voltage plot for 7 and 10 μm cell gap. (d) Electric power consumption in driving a 7 μm thick CNLC cell at different frequencies. (e) Typical dependences of direct transmitted intensity used to determine the response time of CNLC at U_d = 5 V. (f) Rise and decay time versus applied voltage plot. Time taken for output intensity change between 0.9 and 0.1 (two dashed lines) in (e) is used to determine the response times.

through the cell is scattered from the randomly aligned LC director. Similar observations can be made from the uniform conoscopic image of the cell at 0 V, shown in the inset of Figure 4a. Subsequently, as the voltage is increased beyond the threshold voltage level, the LC director within the misaligned domains rotates in response to the applied field, as observed in consecutive conoscopic images (Figure S1c). Finally, at a sufficient voltage, the director is aligned everywhere along the direction of light propagation, resulting in the complete extinction of light under crossed polarizers (Figure S1b). This change in output optical intensity with respect to the applied voltage is used to characterize the threshold voltage (U_{th}) and driving voltage (U_d) for the CNLC cell. As can be noticed from Figure 4a, where the applied voltage is varied in small steps (ΔU = 0.1 V), the threshold voltage U_{th} for a 7 μm thick CNLC cell is found to be about 2.6 V, only slightly higher than that for pure 5CB ($U_{th}^{5CB} \approx 0.8$ V). However, unlike pure LC cells, the threshold voltage for CNLC increases with cell gap (see Figure 4b) which is expected for structured CNLC cells due to the distributed anchoring-based coupling to a 3D network. When measured between crossed polarizers, the output optical intensity becomes extinct around 4.5 V, estimating the value of the driving voltage, U_d. These measurements are also verified from the direct transmittance versus applied voltage plot in Figure 4c, where the cell reaches 10% and 90% of maximum transmission at U_{th} = 2.72 V and U_d = 4.68 V, respectively, for the optimized cell gap of 7 μm. The low driving voltage is a distinctive property of the CNLC switching, considering at least a 1 order of magnitude higher driving voltage of standard PDLC and PSLC composites used recently.[44,45] Such voltage reductions in smart window applications would allow operation with about 100 times lower power requirements, which is approximately proportional to the square of the driving voltage. This order-of-magnitude estimation has been validated experimentally as well. Overall energy consumption for operation and maintaining the "ON" state is found to be about 30−45 mW m^{-2} at a frequency range f = 10−1000 Hz (see Figure 4d), whereas a similar estimation for PDLCs[13,35] is around 5−20 W m^{-2}. The low operating voltages and very steep electro-optic response of the gel are consistent with the weak anchoring conditions of LC molecules as predicted theoretically.[58,59]

To understand the observed threshold field and dynamic switching behavior of CNLC gel, we implemented a model based on considerations of the mechanical coupling between nanofiber network and the LC director.[60] The threshold field from this model (Supporting note 1) for a CNLC gel system with finite anchoring strength can be expressed as

$$E_{th} \cong \sqrt{\frac{2\pi^2 K}{\varepsilon_0 \varepsilon_a}\left(\frac{1}{d} + \frac{1}{L + 2K/W}\right)^2} \quad (1)$$

By replacing the dielectric anisotropy ε_a = 11.5 and average Frank elastic constant $K \approx 5$ pN of 5CB at f = 1000 Hz, ε_0 = 8.85 × 10^{-12} F m^{-1}, U_{th} = 2.74 V for d = 7 μm, and L on the order of 100 nm as seen from the CNF-network electron microscopy image, we get an approximation of the surface anchoring coefficient $W \approx 2.2 \times 10^{-6}$ J m^{-2}. To assess the

https://doi.org/10.1021/acsnano.3c03693
ACS Nano XXXX, XXX, XXX−XXX

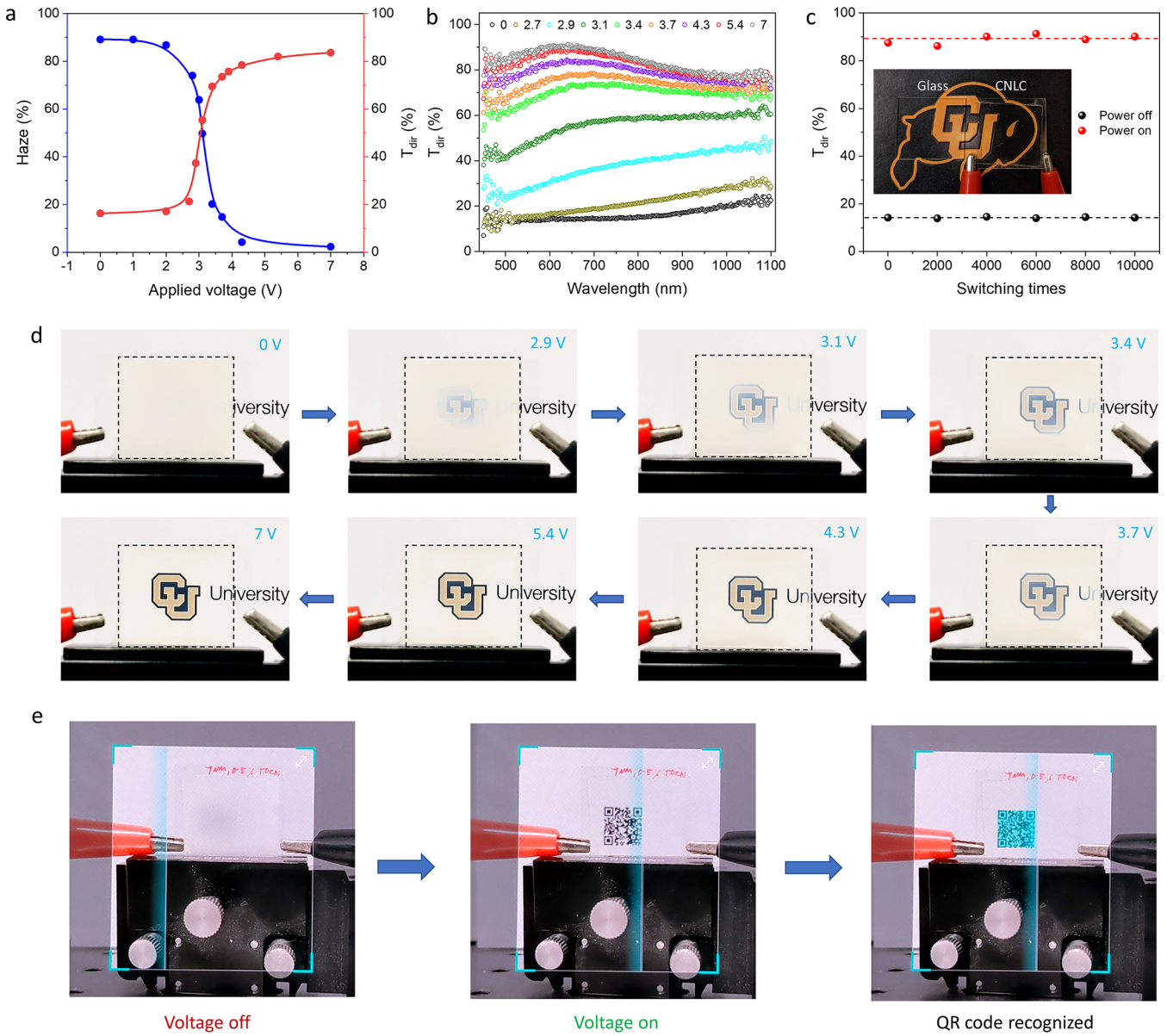

Figure 5. Voltage-dependent optical characterization of the CNLC gel and corresponding demonstrations. (a) Haze coefficient and direct transmittance plot at different voltages. (b) Spectral dependence of direct transmission at different voltage levels. (c) Direct transmittance of the CNLC cell in the OFF state and ON state as a function of number of switching cycles. The appearance of the cell after the final switching cycle in comparison with a cleaned glass substrate is shown in the inset. (d) Photographs of CU logo imaged through the CNLC cell at different voltages. (e) Demonstration of information protection and on-demand detection of a QR code through the CNLC cell. Without the voltage the QR code is blocked, which becomes visible as soon as the voltage is applied. The blue color on the QR code confirms the detection. The copyright of the logos of CU Boulder used in this figure belongs to the University of Colorado at Boulder and their use in this publication is permitted.

validity of our model, we considered the switching response times of the CNLC gel. The threshold field for gel systems is related to the decay time t_{decay} and the rotational viscosity γ by[60] $t_{decay}E_{th}^2 = \frac{\pi^2\gamma}{\varepsilon_0\varepsilon_a}$. So, the decay time can be explicitly written as

$$t_{decay} = \frac{\gamma}{2K}\left(\frac{1}{d} + \frac{1}{L + 2K/W}\right)^{-2} \quad (2)$$

Taking the rotational viscosity of 5CB $\gamma \approx 75$ mPa S at 25 °C and $W \approx 2.2 \times 10^{-6}$ J m^{-2}, found based on our model, the decay time is estimated to be $t_{decay} \approx 57.85$ ms, which we will now verify with experimental measurements on the electrical switching response time of the CNLC gel. Due to weak anchoring to the CNF network, the facile response of 5CB molecules to an applied electric field is fast and comparable to that of a pure LC. With the application of a certain voltage above U_{th}, the optical response of the composite varies nonmonotonously with time as shown in Figure 4e. The rising and decay times are calculated based on the intensity changes of directly transmitted light between 10% and 90%, as marked by dotted lines, obtaining the rising time t_{rise} = 30 ms and decay time t_{decay} = 60 ms, at 5 V in a 7 μm thick cell. With increasing amplitude of the applied voltage, the LC director switches faster, thereby reducing the response time t_{rise}, whereas t_{decay} is independent of the applied voltages as

https://doi.org/10.1021/acsnano.3c03693
ACS Nano XXXX, XXX, XXX−XXX

observed in Figure 4f. The value of t_{decay} from modeling matches closely with the experimentally measured decay time, thereby validating the model and analytical approach overall. These fast switching times, along with low operating voltages, are a key advantage of the CNLC gel for applications such as privacy windows.

Another important optical property to assess the performance of smart glass is the haze coefficient, evaluating the amount of scattered light. In Figure 5a, we quantify the haze coefficient of the ensuing CNLC gels at different voltages from the ratio of the diffused and total transmission. The high haze coefficient (89.49%) at the passive state decreases drastically with applied voltage and finally decreases to a low value of 2.29%, which meets the stringent requirements for the transparent-state properties of glazing. The low haziness of CNLC gels at an applied voltage and the tunability of the haze coefficient with small voltage changes are suitable for applications in privacy windows, daylighting, and skylights. In addition to that, the dependence of direct transmittance on the applied voltage over a broad wavelength range (450−1100 nm) is also revealed. Both of these measurements show threshold-like dependence on the applied voltage, changing rapidly between 2.7 and 4.3 V. From the wavelength dependence of direct transmission in Figure 5b, one observes that the scattering/haze contrast between ON and OFF states is somewhat weaker for NIR wavelengths as compared to the visible range, though still adequate to allow for controlling solar gain also, along with the visible-range transparency. The ability of tuning haze within 2−90% with a very small applied voltage while maintaining the high overall transmission has been highly sought after but not achieved until this work, creating the foundation for our technological approach dubbed "Haze Switch". We also tested the durability of CNLC switching and reproducibility of its performance over various switching cycles. The direct transmittance values at OFF and ON states after every 2000 cycles have been plotted in Figure 5c. The nearly constant response indicates that the CNLC gel is stable over at least 10000 switching cycles and still exhibits ultrahigh ON-state transparency (shown in the inset of Figure 5c). The composite remains reversible at the end of the cycling test, as can be seen from the direct transmission vs wavelength plot in Figure S2. The dynamic modulation for ∼100 switching cycles has been shown in Figure S3, using a square wave electric signal, that verifies the consistency of the optical modulation over multiple switching cycles.

The polarization-independent and color-neutral optical response, along with negligible scattering loss of the CNLC gels, may potentially enable technological advances in smart windows and glasses, polarizer-free information displays, and information security. Finally, we demonstrate the tunability of the visual appearance of the cell with the CU logo under varying voltages in Video S2. The variation of transparency and haziness of the logo image when observed through the CNLC cell at different voltages has been shown in Figure 5d. During the transition, the exact color of the logo remains unaltered. It is interesting to notice that, if the voltage is slowly increased in small steps, the transparency switching starts from the center first and then goes outward. However, this effect is absent when the cell is switched at a constant driving voltage, as observed in Video S1, so that the voltage driving scheme can be optimized for the desired uniformity of switching. A specific example toward an application in information security has been shown in Figure 5e and Video S3, where the CNLC smart glass is used for QR code protection and recognition. CNLC in its passive state always protects the QR code, disabling the smartphone camera to access any (sensitive) information, thereby providing the desired information security. Once the CNLC cell is powered on, the QR code appears and is recognized immediately. This demonstration exhibits that the CNLC cell can act as an additional physical security layer, preventing access to visual information without the end-user authorization on imaging devices connected to the Internet such as smartphone cameras, webcams, and indoor cameras providing Internet of Things (IoT) privacy and security. Similar control should also be possible in machine vision operations for iris recognition and finger-vein biometrics that use the 850−1000 nm near-infrared (NIR) band, owing to the broad-band optical response of the CNLC extending into the NIR wavelengths. The existing securing methods usually have a physical cover, and/or indicator lights[61] whose operation depends on manual action, are often neglected due to various reasons[62] or even can be disabled covertly.[63] There is a growing awareness and concern among users regarding camera privacy.[64] Therefore, a failproof solution is highly desired that can automatically cover a camera when not in use. Pertaining to the micrometer-scale thickness, compatibility with LC display technology, low-voltage operation, and default privacy state, the switchable CNLC gel has the potential to get seamlessly integrated into miniaturized chip-scale devices and coexist with other optical techniques for information security and authentication.[65]

CONCLUSIONS

We have shown that a network of nanocellulose fibers penetrating a nematic liquid crystal allows for switching it between monodomain and polydomain states, where the latter is strongly scattering and the former is highly transparent, with both states providing the high overall transmission of light. The developed CNLC gel enables tuning and fast-switching (millisecond) of the haze coefficient within a broad range, from 2 to ∼90% while maintaining high color-neutral light transmission, leading to the "Haze-Switch" technology that we introduce. We chose CNFs due to their ultrathin diameters and natural abundance and demonstrated use as well as scalability in various technological applications.[66] Other biopolymers such as chitin, chitosan, and nanofibers may also be used, which have much faster processability and easier synthesis than CNFs. Synthetic fibers such as poly(vinyl alcohol) (PVA), polyacrylamide (PAM), and poly(acrylic acid) (PAA) may also be used to form the gel matrix, provided that they can be manufactured to have <10 nm diameters, as needed for the low-haze performance in the clear state. However, one must find the right LC fluid with suitable refractive indices for proper functioning of the gel. Here, we chose the commonly used liquid crystal 5CB, which offers the desired refractive index combinations and is also available in large quantities at a low cost. It is possible to use other known LC materials having RIs similar to that of 5CB, such as E7, but with a higher nematic−isotropic transition temperature which can further be used to achieve a higher operating temperature range. Crucially, the choice of the right combination of RIs is 2-fold for a switchable gel. A strong accessible RI mismatch with respect to the nanofiber network is required for the opaque mode while a near-perfect matching of RIs is desired for the gels to be transparent. It should be possible to modify the CNLC design such that the default state can be transparent

https://doi.org/10.1021/acsnano.3c03693
ACS Nano XXXX, XXX, XXX−XXX

like reverse mode PDLCs, which may be preferred for some applications. For example, a future design can include a combination of vertically aligned CNFs[67] (oriented orthogonally to confining substrates) and an appropriate LC material with negative dielectric anisotropy which reorients perpendicularly to the applied electric field. In this design, initially, when the LC molecules align parallel along the fiber, the gel should appear transparent. The clear mode can then be switched to an opaque mode as soon as the voltage is applied randomizing the LC alignment to form a polydomain structure.

In CNLC gel, the weak surface anchoring of LC molecules on nanometer-thick cellulose fibers leads to randomly aligned emerging nematic domains that control light transport and associated optical diffusion using just a few volts. Due to low operating voltage and electrical power consumption requirements, the gel can be operated by portable devices like a small battery or a compact solar cell without needing extra electrical wiring in the architecture. The electrical voltage requirement may be reduced further by using LC fluids with high dielectric anisotropy or by utilizing nanofibers that, unlike the CNFs, naturally induce weak homeotropic anchoring surface boundary conditions.[68] Additionally, a solar gain control functionality can be potentially added by doping the CNLC gel with plasmonic nanoparticles[69] or dichroic dyes.[70] Moreover, the integration of CNLC with other window technologies based on thermal insulating aerogels[71,72] in a multipane design may offer an all-in-one solution for energy efficiency as well as privacy control while simultaneously allowing natural light which is critical for human health.[73] The CNLC gel uniquely combines high visible transmission (even in the opaque state) and low haze (~2%) in the clear state, as strictly required for window applications.[74,75] The uniformity in color-neutral appearance and selective tuning of polarization-independent haze are also crucial achievements, which are realized through an electrically tunable method. Since the CNLC gel is made from commonly used LC and biopolymer materials, it can be manufactured with minimal expenses and in a highly scalable manner. The fabrication of a CNLC window is very simple, similar to commercially successful PDLCs but like them does not require any of the LC alignment layer, high-temperature processing, UV-illumination, patterning of the LC cell or electrodes, or any other special fabrication scheme that to some extent limits practical window applications. The orders of magnitude reduction of power consumption along with superior switching contrast, stable performance, simple fabrication and operation, reduced expense, and potential scalability make this technology an excellent candidate for realizing the next generations of power-efficient dynamic smart glass which may additionally reduce the building energy consumption from artificial lighting. Devices based on this low-voltage Haze-Switch approach could find applications in various optically switchable technologies, including privacy windows, skylights, sunroofs, daylighting, and information security.

METHODS

Synthesis of TEMPO-Oxidized Cellulose Nanofibers. TEMPO-oxidized individualized cellulose nanofibers were synthesized by a two-step process. In the first step, TEMPO oxidation of demineralized hardwood cellulose pulp (Dragons Paper, Rumford Division, USA) that had never been dried commenced in an alkaline environment at a pH of 10. The process involved adding 100 g of pulp, 28.92 mg of TEMPO (equivalent to 0.094 mmol), and 317.64 mg of NaBr to the suspension, followed by the introduction of 10 mL of 1 M NaClO solution. When the rate of pH reduction was below 0.01 per minute, the solution was transferred to a high-speed blender and mixed for 5−10 min at 1500 rpm. The blending process breaks the aggregated cellulose fibers and allows deeper penetration of the oxidation agent into the interior structures. After blending, the solution was reintroduced to stirring and the pH was readjusted to 10 with 1 M NaOH solution. This procedure was iterated until the solution pH dropped by less than 0.5 following blending. The solution was centrifuged several times at 9000 rpm for 20 min to make it free from excess and unreacted chemicals. This procedure was again reiterated multiple times, with each iteration involving the substitution of waste liquid with deionized water to eliminate any residual chemicals from the solution, leaving behind solely pure oxidized cellulose fibers. Subsequently, the oxidized cellulose nanofibers were retrieved through centrifugation and subjected to extensive washing with water. Following this, they were subjected to another round of mechanical grinding by using a high-speed grinder. The second step started with a sonication for about 15 min using a Branson Sonifier at 30% amplitude. The remaining unreacted C6 hydroxyl groups of cellulose were subsequently oxidized to form C6 carboxylate groups. This oxidation was carried out using $NaClO_2$ as the primary oxidant, along with catalytic quantities of TEMPO and NaClO in a water-based solution at a pH range of 4.8−6.8. Once again, TEMPO facilitated the selective and effective transformation of the C6 hydroxyl groups. To establish a buffer during the reaction, a solution containing 1 M dibasic sodium phosphate (2.35 mL) and 1 M monobasic sodium phosphate (2.65 mL) was introduced to a 1 g solution of TEMPO-oxidized cellulose nanofibers. The mixture was stirred at 500 rpm for about 5 min, after which 20 mL was extracted and kept aside for the purpose of diluting NaClO at a later stage before its addition to the reaction container. Subsequently, TEMPO of 25 mg and $NaClO_2$ of 1.13 g were introduced into the oxidized cellulose nanofiber dispersions, and the mixture was stirred at 500 rpm for around 20 min until these additives were completely dissolved. Next, the previously set aside 20 mL of solution was mixed with NaClO (0.455 mL). After that, the diluted NaClO was incorporated into the cellulose nanofiber dispersion, and the reaction vessel was promptly sealed with a screw lid. The solution was kept within a water bath at room temperature and stirred at a rate of 500 rpm for roughly 30 min. Following this, the water bath's temperature was raised to 60 °C and the reaction proceeded uninterruptedly for a duration of 72 h. Subsequently, the solution underwent multiple rounds of centrifugation at 9000 rpm for 20 min each time to separate and filter out any excess chemicals. In the final step, the dispersion underwent an additional round of sonication using a Branson Sonifier for a duration of 30 min. Following this, the mixture was filtered using Whatman filter paper 2 to obtain the ultimate oxidized cellulose nanofiber dispersion in water. This modified version of the TEMPO oxidation of cellulose results in well-defined rodlike particles, measuring 3−6 nm in width and hundreds to thousands of nanometers length. Moreover, these cellulose nanofibers are mechanically flexible and have high crystallinity, and therefore show strong optical anisotropy.

Fabrication of the CNLC Cells As Haze-Switch Devices. Aqueous dispersions of the synthesized nanofibers with concentrations of 0.5−1 wt % were mixed with silica spacers of desired thickness ranging from 4 to 15 μm. A few drops of this mixture were drop-cast on a desired substrate. Subsequently, another substrate was placed on top, which was then glued to the other substrate with UV-curable NOA-65 glue (Norland Products, Inc.) and formed a uniformly thick cell with the desired cell gap. To initiate gelation, the cell was then immersed overnight in a weak acid solution made from 5 wt % acetic acid. During this step, the fibers were cross-linked to form a 3D network. Once the gelation was completed, the cell was transferred to a water bath and kept at room temperature for another 2 days to wash out the acid. Later, the ensuing hydrogel was dipped in ethanol and kept at 50 °C for 1 day for solvent exchange. At last, the CNLC was formed by replacing ethanol from the network with 5CB (Chengzhi Yonghua Display Materials Co. Ltd.) at 60 °C for 3 days.

https://doi.org/10.1021/acsnano.3c03693
ACS Nano XXXX, XXX, XXX−XXX

During the solvent exchange process, which turned the hydrogel into an alcogel and finally into the desired CNLC gel, the fiber network remained unperturbed as we avoided the use of any solvent that could possibly break the hydrogen bonds linking the fibers. We have not noticed any separation between the LC and the CNF network or any aggregation of the LC even after several months since their fabrication. Moreover, the CNLC gels were switched months apart, but their performance showed no detectable differences. Also, during our experiments we have not observed any Joule heating side effects such as drying or degradation of the gel even after 10000 switching cycles. The negligible Joule heating can be attributed to the low operating voltage and frequencies as well as to the capacitive (dielectric, with low conductivity) nature of the CNLC cells.

Nanoscale Characterization. Transmission electron microscopy (TEM) characterization of the fibers and the ensuing network was done by capturing the tilt series on a Titan Krios G3i at 300 kV under low-dose conditions. The SerialEM program was employed for the acquisition of the tilt series data, while the IMOD software was utilized for the reconstruction of the tomographic data.[76] The individualized cellulose nanofibers in aqueous dispersions underwent negative staining with 1% phosphotungstic acid before being imaged using a Tecnai ST20 200 kV transmission electron microscope. To avoid any possibility of modifications to the internal structure during transfers and processing, thin films of the nanofiber network were fabricated directly on TEM grids with 300 mesh Au carbon coating, enabling direct imaging.

Electro-optical Characterization. The total and diffused transmission spectra within the visible range (400−800 nm) were taken by using a spectrometer in conjunction with an integrating sphere (Labsphere DRA-CA-5500) having an internal diameter of 150 mm and coated with barium sulfate. The haze coefficient, which measures the extent of scattered light, was determined using integrating sphere measurements of total and diffused transmission. These calculations were performed in accordance with ASTM D1003 (Standard Test Method for Haze and Luminous Transmittance), a widely adopted standard for quantifying haze in window applications. To measure optical transmittance and haze coefficients, the samples were affixed at the entrance of the integrating sphere and calibration was executed using standards for diffuse reflectance. The direct transmission spectra in the 400−1100 nm wavelength range were studied by using a portable spectrometer (Silver Nova, from Stellernet Inc.) mounted on the microscope. Broad-spectrum light was collected and analyzed using an optical fiber having a core diameter of 600 μm. The optical microscopy observations were performed using an Olympus BX-51 upright optical microscope equipped with a 10× and 50× air objective of numerical aperture 0.3 and a charge-coupled device (CCD) camera (Pointgrey).

The characterization of the composite's electrical switching was conducted using a data acquisition system (National Instruments Co., USB-6259) managed by custom software developed in LabVIEW (National Instruments Co.), in conjunction with a silicon-amplified photodetector (Thorlabs Inc., PDA100A2). A function generator (Instek GFG-8216A) was used as the voltage source at different frequencies. We used a Schlumberger 1260 Impedance gain-phase analyzer with a maximum input voltage of 3 V for measuring power consumption.

Estimation of Power Consumption. To study the power consumption of the CNLC cell as a function of frequency, the impedance (magnitude and phase) of the cell was measured. We used a typical cell of thickness d = 7 μm and electrode area A = 6.45 cm^2 for the measurements. The sample was scanned over a range of operating frequencies from 10 Hz to 1 kHz at an applied voltage of 3 V. Now, the average dissipated power in ac circuits can be found from $P_{avg} = \frac{V_m^2}{2Z} \cos \varphi$, where V_m is the applied voltage, Z is the impedance of the circuit, and φ is the phase angle between voltage and current.

ASSOCIATED CONTENT

Supporting Information

The Supporting Information is available free of charge at https://pubs.acs.org/doi/10.1021/acsnano.3c03693.

Analytical model for the threshold field, orthoscopic and conoscopic images of the CNLC gel, direct transmission vs wavelength plot after 10000 switching cycles, and transmission modulation over ∼100 switching cycles (PDF)

Demonstration of the transparency-switching CNLC smart glass, changing between the hazy OFF-state and transparent ON-state multiple times (AVI)

Demonstration of tunable haze with varying voltages (AVI)

Demonstration of QR code scanning and detection (AVI)

AUTHOR INFORMATION

Corresponding Authors

Ivan I. Smalyukh − *Department of Physics, University of Colorado, Boulder, Colorado 80309, United States; International Institute for Sustainability with Knotted Chiral Meta Matter (WPI-SKCM^2), Hiroshima University, Boulder, Higashihiroshima 739-8526, Japan; Renewable and Sustainable Energy Institute, National Renewable Energy Laboratory and University of Colorado, Boulder, Colorado 80309, United States;* orcid.org/0000-0003-3444-1966; Email: ivan.smalyukh@colorado.edu

Souvik Ghosh − *Department of Physics, University of Colorado, Boulder, Colorado 80309, United States;* orcid.org/0000-0001-9428-7193; Email: souvik.ghosh@colorado.edu

Author

Eldho Abraham − *Department of Physics, University of Colorado, Boulder, Colorado 80309, United States*

Complete contact information is available at: https://pubs.acs.org/10.1021/acsnano.3c03693

Author Contributions

I.I.S. conceived this project. S.G. planned the experimental methodology, performed experimental studies, and analyzed data. E.A. synthesized the cellulose nanofibers and provided TEM characterizations. S.G. and I.I.S. wrote the manuscript with input from all authors.

Funding

This research was supported by the US Department of Energy, Office of Basic Energy Sciences, Division of Materials Sciences and Engineering, under contract DE-SC0019293 with the University of Colorado at Boulder.

Notes

The authors declare no competing financial interest.

ACKNOWLEDGMENTS

We acknowledge the discussions and technical assistance of B. Senyuk, P. de Melo, and J. B. ten Hove. I.I.S. acknowledges hospitality of the international Institute for Sustainability with Knotted Chiral Meta Matter (SKCM^2) at Hiroshima University and the Biosoft Centre at Tel Aviv University during his sabbatical visits, where he was partly working on this article.

ABBREVIATIONS

LC, liquid crystal; CNLC, cellulose network liquid crystals; PDLC, polymer-dispersed liquid crystals; PSLC, polymer-stabilized liquid crystals; TOCN, TEMPO-oxidized cellulose nanofibers

REFERENCES

(1) Ishimaru, A. *Wave Propagation and Scattering in Random Media*; Academic Press: New York, 1978; Vol. 2.

(2) Bohren, C. F.; Huffman, D. R. *Absorption and Scattering of Light by Small Particles*; Wiley & Sons: Weinheim, 1998.

(3) Hulst, H. C.; van de Hulst, H. C. *Light Scattering by Small Particles*; Dover Publications: New York, 1981.

(4) Carminati, R.; Schotland, J. C. *Principles of Scattering and Transport of Light*; Cambridge University Press: New York, 2021.

(5) Rotter, S.; Gigan, S. Light Fields in Complex Media: Mesoscopic Scattering Meets Wave Control. *Rev. Mod. Phys.* **2017**, *89* (1), 15005.

(6) Wiersma, D. S. Disordered Photonics. *Nat. Photonics* **2013**, *7* (3), 188−196.

(7) Kolle, M.; Lee, S. Progress and Opportunities in Soft Photonics and Biologically Inspired Optics. *Adv. Mater.* **2018**, *30* (2), 1702669.

(8) Zhou, L.; Liu, S.; Zhong, T. A Comprehensive Review of Optical Diffusers: Progress and Prospect. *Nanoscale* **2023**, *15*, 1484−1492.

(9) Timmermans, G. H.; Hemming, S.; Baeza, E.; van Thoor, E. A. J.; Schenning, A. P. H. J.; Debije, M. G. Advanced Optical Materials for Sunlight Control in Greenhouses. *Adv. Opt Mater.* **2020**, *8* (18), 2000738.

(10) Brongersma, M. L.; Cui, Y.; Fan, S. Light Management for Photovoltaics Using High-Index Nanostructures. *Nat. Mater.* **2014**, *13* (5), 451−460.

(11) Wang, W.; Qi, L. Light Management with Patterned Micro- and Nanostructure Arrays for Photocatalysis, Photovoltaics, and Optoelectronic and Optical Devices. *Adv. Funct Mater.* **2019**, *29* (25), 1807275.

(12) Haghanifar, S.; Galante, A. J.; Leu, P. W. Challenges and Prospects of Bio-Inspired and Multifunctional Transparent Substrates and Barrier Layers for Optoelectronics. *ACS Nano* **2020**, *14* (12), 16241−16265.

(13) Shrestha, M.; Lau, G. K.; Bastola, A. K.; Lu, Z.; Asundi, A.; Teo, E. H. T. Emerging Tunable Window Technologies for Active Transparency Tuning. *Appl. Phys. Rev.* **2022**, *9* (3), 031304.

(14) Ke, Y.; Chen, J.; Lin, G.; Wang, S.; Zhou, Y.; Yin, J.; Lee, P. S.; Long, Y. Smart Windows: Electro-, Thermo-, Mechano-, Photochromics, and Beyond. *Adv. Energy Mater.* **2019**, *9* (39), 1902066.

(15) Shen, W.; Li, G. Recent Progress in Liquid Crystal-Based Smart Windows: Materials, Structures, and Design. *Laser Photon Rev.* **2023**, *17* (1), 2200207.

(16) Fang, Z.; Zhu, H.; Bao, W.; Preston, C.; Liu, Z.; Dai, J.; Li, Y.; Hu, L. Highly Transparent Paper with Tunable Haze for Green Electronics. *Energy Environ. Sci.* **2014**, *7* (10), 3313−3319.

(17) Pafchek, B.; Leu, P. W.; Vecchis, R. T. R. De; Haghanifar, S.; Jacobs, T. D. B.; Gao, T. Ultrahigh-Transparency, Ultrahigh-Haze Nanograss Glass with Fluid-Induced Switchable Haze. *Optica* **2017**, *4* (12), 1522−1525.

(18) Jacucci, G.; Schertel, L.; Zhang, Y.; Yang, H.; Vignolini, S. Light Management with Natural Materials: From Whiteness to Transparency. *Advanced materials* **2021**, *33* (28), 2001215.

(19) Liu, Q.; Frazier, A. W.; Zhao, X.; Joshua, A.; Hess, A. J.; Yang, R.; Smalyukh, I. I. Flexible Transparent Aerogels as Window Retrofitting Films and Optical Elements with Tunable Birefringence. *Nano Energy* **2018**, *48*, 266−274.

(20) Zeng, Z.; Mavrona, E.; Sacre, D.; Kummer, N.; Cao, J.; Müller, L. A. E.; Hack, E.; Zolliker, P.; Nyström, G. Terahertz Birefringent Biomimetic Aerogels Based on Cellulose Nanofibers and Conductive Nanomaterials. *ACS Nano* **2021**, *15* (4), 7451−7462.

(21) Zhao, Z.; Fang, R.; Rong, Q.; Liu, M. Bioinspired Nanocomposite Hydrogels with Highly Ordered Structures. *Adv. Mater.* **2017**, *29* (45), 1703045.

(22) Kong, W.; Wang, C.; Jia, C.; Kuang, Y.; Pastel, G.; Chen, C.; Chen, G.; He, S.; Huang, H.; Zhang, J.; et al. Muscle-inspired Highly Anisotropic, Strong, Ion-conductive Hydrogels. *Adv. Mater.* **2018**, *30* (39), 1801934.

(23) Crawford, G. P.; Zumer, S. *Liquid Crystals in Complex Geometries: Formed by Polymer and Porous Networks*; Taylor & Francis: London, 1996.

(24) Zhang, H.; Miao, Z.; Shen, W. Development of Polymer-Dispersed Liquid Crystals: From Mode Innovation to Applications. *Compos Part A Appl. Sci. Manuf* **2022**, *163*, 107234.

(25) Zhang, R.; Zhang, Z.; Han, J.; Yang, L.; Li, J.; Song, Z.; Wang, T.; Zhu, J. Advanced Liquid Crystal-Based Switchable Optical Devices for Light Protection Applications: Principles and Strategies. *Light Sci. Appl.* **2023**, *12* (1), 11.

(26) Doane, J. W.; Vaz, N. A.; Wu, B. G.; Žumer, S. Field Controlled Light Scattering from Nematic Microdroplets. *Appl. Phys. Lett.* **1986**, *48* (4), 269−271.

(27) Fergason, J. L. Polymer Encapsulated Nematic Liquid Crystals for Display and Light Control Applications. *SID Dig. Technol. Paper* **1985**, *16*, 68−70.

(28) Dierking, I. Polymer Network ± Stabilized Liquid Crystals**. *Adv. Mater.* **2000**, *12* (3), 167−181.

(29) Meng, C.; Tseng, M. C.; Tang, S. T.; Zhao, C. X.; Yeung, S. Y.; Kwok, H. S. Normally Transparent Smart Window with Haze Enhancement via Inhomogeneous Alignment Surface. *Liq Cryst.* **2019**, *46* (3), 484−491.

(30) Hu, X.; Zhang, X.; Yang, W.; Jiang, X. F.; Jiang, X.; de Haan, L. T.; Yuan, D.; Zhao, W.; Zheng, N.; Jin, M.; Shui, L.; Schenning, A. P. H. J.; Zhou, G. Stable and Scalable Smart Window Based on Polymer Stabilized Liquid Crystals. *J. Appl. Polym. Sci.* **2020**, *137* (30), 48917.

(31) Ren, H.; Wu, S.-T. Reflective Reversed-Mode Polymer Stabilized Cholesteric Texture Light Switches. *J. Appl. Phys.* **2002**, *92* (2), 797−800.

(32) Liu, Q.; Smalyukh, I. I. Liquid Crystalline Cellulose-Based Nematogels. *Sci. Adv.* **2017**, *3* (8), No. e1700981.

(33) Kato, T.; Hirai, Y.; Nakaso, S.; Moriyama, M. Liquid-Crystalline Physical Gels. *Chem. Soc. Rev.* **2007**, *36* (12), 1857−1867.

(34) Baetens, R.; Jelle, B. P.; Gustavsen, A. Properties, Requirements and Possibilities of Smart Windows for Dynamic Daylight and Solar Energy Control in Buildings: A State-of-the-Art Review. *Sol. Energy Mater. Sol. Cells* **2010**, *94* (2), 87−105.

(35) Casini, M. Active Dynamic Windows for Buildings: A Review. *Renew Energy* **2018**, *119*, 923−934.

(36) Doane, J. W.; Golemme, A.; West, J. L.; Whitehead Jr, J. B.; Wu, B.-G. Polymer Dispersed Liquid Crystals for Display Application. *Mol. Cryst. Liq. Cryst.* **1988**, *165* (1), 511−532.

(37) Drzaic, P. S. Polymer Dispersed Nematic Liquid Crystal for Large Area Displays and Light Valves. *J. Appl. Phys.* **1986**, *60* (6), 2142−2148.

(38) Ge, D.; Lee, E.; Yang, L.; Cho, Y.; Li, M.; Gianola, D. S.; Yang, S. A Robust Smart Window: Reversibly Switching from High Transparency to Angle-independent Structural Color Display. *Adv. Mater.* **2015**, *27* (15), 2489−2495.

(39) Birch, E. E. Amblyopia and Binocular Vision. *Prog. Retin Eye Res.* **2013**, *33* (1), 67−84.

(40) Wang, J.; Neely, D. E.; Galli, J.; Schliesser, J.; Graves, A.; Damarjian, T. G.; Kovarik, J.; Bowsher, J.; Smith, H. A.; Donaldson, D.; Haider, K. M.; Roberts, G. J.; Sprunger, D. T.; Plager, D. A. A Pilot Randomized Clinical Trial of Intermittent Occlusion Therapy Liquid Crystal Glasses versus Traditional Patching for Treatment of Moderate Unilateral Amblyopia. *Journal of American Association for Pediatric Ophthalmology and Strabismus* **2016**, *20* (4), 326−331.

(41) Do, Y.; Park, J. W.; Wu, Y.; Basu, A.; Zhang, D.; Abowd, G. D.; Das, S. Smart Webcam Cover. *Proc. ACM Interact Mob Wearable Ubiquitous Technol.* **2021**, *5* (4), 1−21.

(42) Wu, B.-G.; Erdmann, J. H.; Doane, J. W. Response Times and Voltages for PDLC Light Shutters. *Liq Cryst.* **1989**, *5* (5), 1453−1465.

https://doi.org/10.1021/acsnano.3c03693
ACS Nano XXXX, XXX, XXX−XXX

(43) Saeed, M. H.; Zhang, S.; Cao, Y.; Zhou, L.; Hu, J.; Muhammad, I.; Xiao, J.; Zhang, L.; Yang, H. Recent Advances in the Polymer Dispersed Liquid Crystal Composite and Its Applications. *Molecules* **2020**, *25* (23), 5510.
(44) Murray, J.; Ma, D.; Munday, J. N. Electrically Controllable Light Trapping for Self-Powered Switchable Solar Windows. *ACS Photonics* **2017**, *4* (1), 1−7.
(45) Wang, J.; Meng, C.; Gu, Q.; Tseng, M. C.; Tang, S. T.; Kwok, H. S.; Cheng, J.; Zi, Y. Normally Transparent Tribo-Induced Smart Window. *ACS Nano* **2020**, *14* (3), 3630−3639.
(46) Chen, Y. H.; Lin, P. Y.; Wang, T. W.; Tiwari, N.; Lin, S. C.; Wu, H. S.; Choi, D.; Wu, W.; Choi, D.; Hsiao, Y. C.; Lin, Z. H. Dynamics of Electrically Driven Cholesteric Liquid Crystals by Triboelectrification and Their Application in Self-Powered Information Securing and Vision Correcting. *ACS Energy Lett.* **2021**, *6* (9), 3185−3194.
(47) Wang, J.; Meng, C.; Wang, C.-T.; Liu, C.-H.; Chang, Y.-H.; Li, C.-C.; Tseng, H.-Y.; Kwok, H.-S.; Zi, Y. A Fully Self-Powered, Ultra-Stable Cholesteric Smart Window Triggered by Instantaneous Mechanical Stimuli. *Nano Energy* **2021**, *85*, 105976.
(48) Li, Y.; Wang, M.; Zhang, C.; Wang, C. C.; Xu, W.; Gao, S.; Zhou, Y.; Wang, C. T.; Wang, Z. A Fully Self-Powered Cholesteric Smart Window Actuated by Droplet-Based Electricity Generator. *Adv. Opt Mater.* **2022**, *10* (7), 2102274.
(49) Fukuzumi, H.; Tanaka, R.; Saito, T.; Isogai, A. Dispersion Stability and Aggregation Behavior of TEMPO-Oxidized Cellulose Nanofibrils in Water as a Function of Salt Addition. *Cellulose* **2014**, *21* (3), 1553−1559.
(50) Isogai, A.; Saito, T.; Fukuzumi, H. TEMPO-Oxidized Cellulose Nanofibers. *Nanoscale* **2011**, *3* (1), 71−85.
(51) Lagerwall, J. P. F.; Schütz, C.; Salajkova, M.; Noh, J.; Hyun Park, J.; Scalia, G.; Bergström, L. Cellulose Nanocrystal-Based Materials: From Liquid Crystal Self-Assembly and Glass Formation to Multifunctional Thin Films. *NPG Asia Mater.* **2014**, *6* (1), No. e80.
(52) Li, T.; Chen, C.; Brozena, A. H.; Zhu, J. Y.; Xu, L.; Driemeier, C.; Dai, J.; Rojas, O. J.; Isogai, A.; Wågberg, L.; et al. Developing Fibrillated Cellulose as a Sustainable Technological Material. *Nature* **2021**, *590* (7844), 47−56.
(53) Klemm, D.; Philpp, B.; Heinze, T.; Heinze, U.; Wagenknecht, W. *Comprehensive Cellulose Chemistry. Volume 1: Fundamentals and Analytical Methods*; Wiley-VCH Verlag GmbH: Weinheim, 1998.
(54) Wu, S.-T.; Wu, C.; Warenghem, M.; Ismaili, M. Refractive Index Dispersions of Liquid Crystals. *Optical Engineering* **1993**, *32* (8), 1775−1780.
(55) Lavrentovich, O. D.; Palffy-Muhoray, P. Scientific Note: Nematic Structures in Composite Materials. *Liquid crystals today* **1995**, *5* (2), 5−6.
(56) Imry, Y.; Ma, S. Random-Field Instability of the Ordered State of Continuous Symmetry. *Phys. Rev. Lett.* **1975**, *35* (21), 1399.
(57) Hikmet, R. A. M. Electrically Induced Light Scattering from Anisotropic Gels. *J. Appl. Phys.* **1990**, *68* (9), 4406−4412.
(58) Nehring, J.; Kmetz, A. R.; Scheffer, T. J. Analysis of Weak-Boundary-Coupling Effects in Liquid-Crystal Displays. *J. Appl. Phys.* **1976**, *47* (3), 850−857.
(59) De Gennes, P.-G.; Prost, J. *Physics of Liquid Crystals*; Oxford University Press: New York, 1993.
(60) Kossyrev, P. A.; Qi, J.; Priezjev, N. V.; Pelcovits, R. A.; Crawford, G. P. Virtual Surfaces, Director Domains, and the Freedericksz Transition in Polymer-Stabilized Nematic Liquid Crystals. *Appl. Phys. Lett.* **2002**, *81* (16), 2986−2988.
(61) Portnoff, R. S.; Lee, L. N.; Egelman, S.; Mishra, P.; Leung, D.; Wagner, D. Somebody's Watching Me? Assessing the Effectiveness of Webcam Indicator Lights. In *Proceedings of the 33rd Annual ACM Conference on Human Factors in Computing Systems*; 2015; pp 1649−1658.
(62) Machuletz, D.; Laube, S.; Böhme, R. Webcam Covering as Planned Behavior. In *Proceedings of the 2018 CHI Conference on Human Factors in Computing Systems*; 2018; pp 1−13.
(63) Brocker, M.; Checkoway, S. ISeeYou: Disabling the MacBook Webcam Indicator LED. In *Proceedings of the 23rd USENIX Security Symposium*; 2014; pp 337−352.
(64) Balthrop, J. *HP Survey highlights webcam security and privacy behaviors*. https://press.hp.com/us/en/press-releases/2019/awareness-of-webcam-hacking.html. Accessed on February 17, 2023.
(65) Matoba, O.; Nomura, T.; Perez-Cabre, E.; Millan, M. S.; Javidi, B. Optical Techniques for Information Security. *Proceedings of the IEEE* **2009**, *97* (6), 1128−1148.
(66) Zhu, H.; Luo, W.; Ciesielski, P. N.; Fang, Z.; Zhu, J. Y.; Henriksson, G.; Himmel, M. E.; Hu, L. Wood-Derived Materials for Green Electronics, Biological Devices, and Energy Applications. *Chem. Rev.* **2016**, *116* (16), 9305−9374.
(67) Li, K.; Clarkson, C. M.; Wang, L.; Liu, Y.; Lamm, M.; Pang, Z.; Zhou, Y.; Qian, J.; Tajvidi, M.; Gardner, D. J.; et al. Alignment of Cellulose Nanofibers: Harnessing Nanoscale Properties to Macroscale Benefits. *ACS Nano* **2021**, *15* (3), 3646−3673.
(68) Aguirre, L. E.; de Oliveira, A.; Seč, D.; Čopar, S.; Almeida, P. L.; Ravnik, M.; Godinho, M. H.; Žumer, S. Sensing Surface Morphology of Biofibers by Decorating Spider Silk and Cellulosic Filaments with Nematic Microdroplets. *Proc. Natl. Acad. Sci. U. S. A.* **2016**, *113* (5), 1174−1179.
(69) Ghosh, S.; Smalyukh, I. Electrical Switching of Nematic Plasmonic Nanocolloids for Infrared Solar Gain Control. *Adv. Opt Mater.* **2022**, *10* (20), 2201513.
(70) Shen, W.; Zhang, H.; Miao, Z.; Ye, Z. Recent Progress in Functional Dye-Doped Liquid Crystal Devices. *Adv. Funct Mater.* **2023**, *33* (6), 2210664.
(71) Smalyukh, I. I. Thermal Management by Engineering the Alignment of Nanocellulose. *Adv. Mater.* **2021**, *33* (28), 2001228.
(72) Abraham, E.; Cherpak, V.; Senyuk, B.; ten Hove, J. B.; Lee, T.; Liu, Q.; Smalyukh, I. I. Highly Transparent Silanized Cellulose Aerogels for Boosting Energy Efficiency of Glazing in Buildings. *Nat. Energy* **2023**, *8*, 381.
(73) Juzeniene, A.; Brekke, P.; Dahlback, A.; Andersson-Engels, S.; Reichrath, J.; Moan, K.; Holick, M. F.; Grant, W. B.; Moan, J. Solar Radiation and Human Health. *Rep. Prog. Phys.* **2011**, *74* (6), 066701.
(74) Carmody, J.; Selkowitz, S.; Lee, E.; Arasteh, D.; Willmert, T. *Window System for High-Performance Buildings*. W. W. Norton: New York, 2004.
(75) Bansal, N. K.; Mathur, J. *Energy Efficient Windows*; Anamaya Publishers: New Delhi, 2006.
(76) Mastronarde, D. N. SerialEM: A Program for Automated Tilt Series Acquisition on Tecnai Microscopes Using Prediction of Specimen Position. *Microscopy and Microanalysis* **2003**, *9* (S02), 1182−1183.

https://doi.org/10.1021/acsnano.3c03693
ACS Nano XXXX, XXX, XXX−XXX